ARTICLES

Volcanic earthquakes at Pavlof Volcano correlated with the solid earth tide

S. R. McNutt* and R. J. Beavan†

*Department of Geological Sciences, Columbia University and †Lamont-Doherty Geological Observatory of Columbia University, Palisades, New York 10964, USA

Volcanic earthquake swarms at Pavlof Volcano, Alaska, correlate significantly with solid earth tidal stress rate for periods just before and just after explosive eruptions. The correlation changes sign systematically during the course of the 1974 minor eruption sequence; pre-eruptive earthquake swarms occur during increasing tidal compression, while post-eruptive swarms occur during increasing tidal extension.

IT has been proposed that the solid earth tide has a role in triggering both earthquakes and volcanic eruptions (see refs 1–5). Crustal stresses of the solid earth tide are of the order of 0.03 bar, with principal periods of ~12 h 25 min, 24 h 50 min, and 14.7 days, and constitute some of the largest pervasive short period oscillatory stresses in the Earth's crust[6]. We examine here the relationship between volcanic microearthquakes and the solid earth tide during the autumn 1974 minor eruption of Pavlof Volcano, Alaska. A correlation has been found between B-type[7] volcanic earthquake swarms and solid earth tidal stress for periods of 3–4 days before and after eruptions. The correlation changes sign systematically for time periods before and after the eruptions, corresponding to periods of presumed inflation and deflation of the volcano.

Pavlof is a 2,715-m high stratovolcano located near the end of the Alaska Peninsula at 55°25′ N, 161°54′ W. It is one of the most active volcanoes in North America with at least 27 documented eruptions since 1700 (S. Hickman, personal communication). Strombolian eruptive activity typically includes lava fountaining and flows, emission of steam and ash, and minor explosions. Analysed lavas are basalt, with small phenocrysts of plagioclase, olivine, hypersthene and augite[8]. The upper portion of the mountain is covered by glaciers.

Twelve seismometers are in operation near Pavlof (Fig. 1). BLH and PVV are stations of the Shumagin Islands regional network, operated since 1973 by Lamont-Doherty in cooperation with the University of Alaska. The remaining local network stations were installed by Lamont-Doherty in 1976, that is, after the sequence of eruptions discussed here. Most of the data presented here are from station PVV, a short period (1 Hz) vertical seismometer located adjacent to an old lava flow 7.5 km south-east of the volcano's summit. The data are recorded on paper helicorder records.

The autumn 1974 eruption sequence began with minor explosive activity from 2 to 21 September, followed by a period of repose. Explosive activity occurred again from 29 October to 19 November, 25 November to 16 December and 25 December to 6 January. Each of these three periods of explosive volcanism began 3–4 days after fortnightly neap tides, in close agreement with Johnston and Mauk's previous results from Mt Stromboli, Italy[9].

Table 1 Pavlof volcano seismicity

Period	Mean no. of events per 2 h	s.d.	No. of data points
Non-eruptive	10.05	5.65	96
Pre-eruptive	26.74	18.81	114
Eruptive	20.24	13.58	178
Post-eruptive	14.19	13.53	161

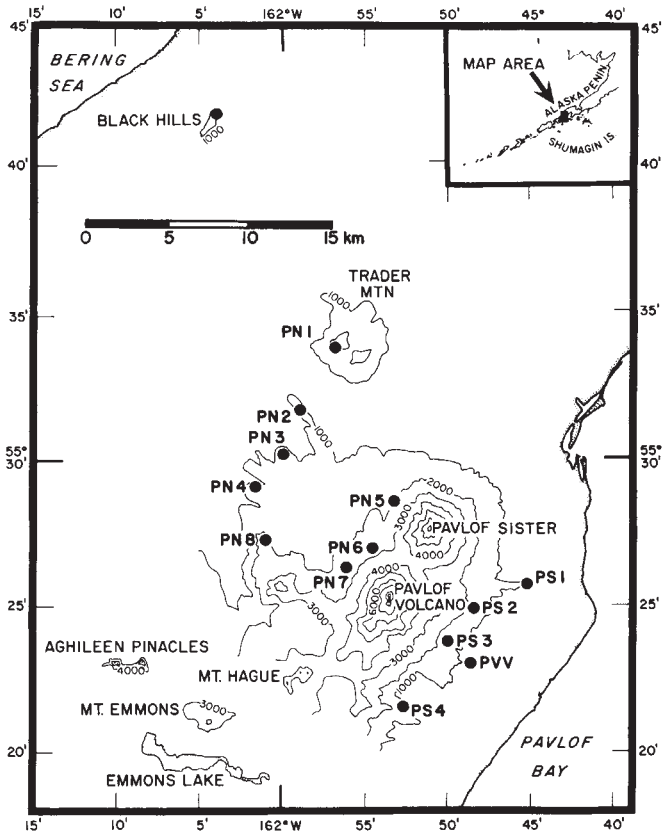

Fig. 1 Map showing stations of the Pavlof seismic array. Data are from station PVV, 7.5 km to the south-east of the volcano's summit.

Seismicity

Data reduction consisted of detailed counts of each of four different types of volcanic earthquakes: high frequency tremors, harmonic tremor, explosion earthquakes and B-type earthquakes ranging in magnitude from −0.2 to 1.0 (Fig. 2) (S. McNutt in preparation). The numbers of events of each type per 2-h interval were plotted on histograms (see Fig. 3) for the entire time period from 1 September 1974 to 30 April 1975. Table 1 gives statistics for the general seismicity, broken down into four periods: non-eruptive (background), pre-eruptive, eruptive and post-eruptive. Seismicity is highest during pre-eruptive periods, followed by eruptive, post-eruptive, and background periods.

0028-0836/81/510615—04$01.00

Table 2 Number of B-type events versus tidal stress rates in certain azimuths

	Azimuth	0°	45°	90°	135°	Volumetric	N
Non-eruptive	14–16 January	0.17	0.19	0.19	0.14	0.20	36
		−0.21	+0.04	−0.46	−0.22	−0.26	
		—	—	—	—	—	
Eruptive	4–8 November	0.02	0.11	0.09	0.00	0.05	42
		−0.04	+0.01	−0.26	0.00	−0.11	
		—	—	—	—	—	
Pre-eruptive	29 October–1 November	0.45	0.49	0.49	0.41	0.51*	37
		−1.24	−1.67	−2.48	−1.45	−1.50	
		99%	99%	99%	99%	99.9%	
Post-eruptive	18–21 November	0.22	0.22	0.33	0.31	0.29	46
		+0.50	+0.56	+0.86	+0.72	+0.56	
		—	—	98%	95%	95%	
Pre-eruptive	22–26 November	0.25	0.32	0.38	0.26	0.33	43
		−0.82	−1.25	−2.16	−1.05	−1.10	
		—	95%	98%	—	95%	
Post-eruptive	7–12 January	0.35	0.36	0.34	0.32	0.37*	60
		+0.93	+1.09	+1.26	+0.98	+0.93	
		99%	99%	99%	98%	99%	

The upper value of each entry is the correlation coefficient, the second is the normalized slope and the third is the confidence level estimate for those cases where it is greater than 90%. N is the number of data pairs used.

* The data plotted in Fig. 4.

Eruptive periods are so designated on the basis of the presence of explosive activity.

B-type earthquakes (Fig. 2) at Pavlof are nearly identical to those observed elsewhere[7,10]. They have emergent onsets, no clear S-phases, dominant frequencies of ~1.4 Hz, and coda durations of ~20 s. Other studies in Japan[7] have located B-type earthquakes at extremely shallow depths (1 km) immediately adjacent to active vents. The Gutenberg–Richter magnitude frequency relation for 1,316 B-type earthquakes which took place from 1 to 8 December has a negative slope or b-value of 2.6 ± 0.2, in close accord with values calculated for other volcanoes[7,10,11]. Explosion earthquakes (Fig. 2) closely resemble B-type earthquakes, except for an impulsive spike ~21 s after the signal onset. This spike is the air shock phase.

Tidal computations

The earthquake histograms were compared with a synthetic solid earth horizontal stress tide in azimuths 0°–180° and with volumetric stress. The components of the tide as a function of time and position were calculated by Longman's method[12], using a program which agrees closely with independent computations. Longman's method calculates tidal potential, from which stress is easily derived by differentiating and using the stress–strain relations with standard values of Love numbers and Lamé parameters. Visual inspection showed that earthquakes tended to occur at times of increasing or decreasing stress in certain azimuths. We therefore differentiated the synthetic stress tides with respect to time to generate stress rate tides (Fig. 3).

The ocean loading tide must be accounted for as well as the solid earth tide; for the particular case of Pavlof, the ocean load stress tide is approximately in phase with the solid earth tide. A rough calculation using Farrell's[13] Green's functions and Schwiderski's[14] ocean tide charts shows that for volumetric stress and for stress in azimuth N90° E the load tide maxima are within 1 h of the solid earth tide maxima. The load tide amplitude is ~30% that of the solid earth tide; hence the inclusion of the load tide changes the phase by <1 h. We do not consider here the detailed effect of topography on the stress tide, but note that topography normally has a small effect on the phase[15].

Correlation data

Linear correlation coefficients between number of earthquakes per 2 h period and tidal stress rate for 15° increments in azimuth were calculated for portions of the eruption sequence. Figure 3 shows the number of earthquakes and two components of stress rate plotted against time for two pre-eruptive and two post-eruptive portions of the data. The third post and pre-eruptive

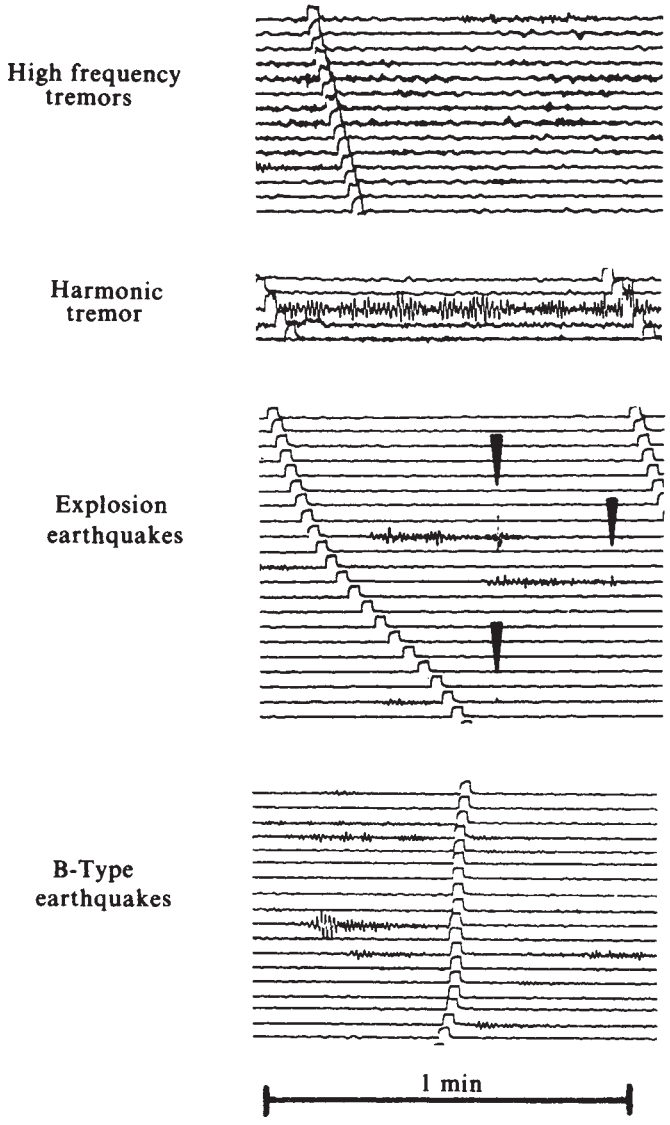

Fig. 2 Types of seismic signals recorded on helicorder from station PVV. Arrows point to air shock phase of explosion earthquakes. Note the similar frequency content (≈1.4 Hz) of B-type earthquakes, harmonic tremor, and ground waves from the explosion earthquakes.

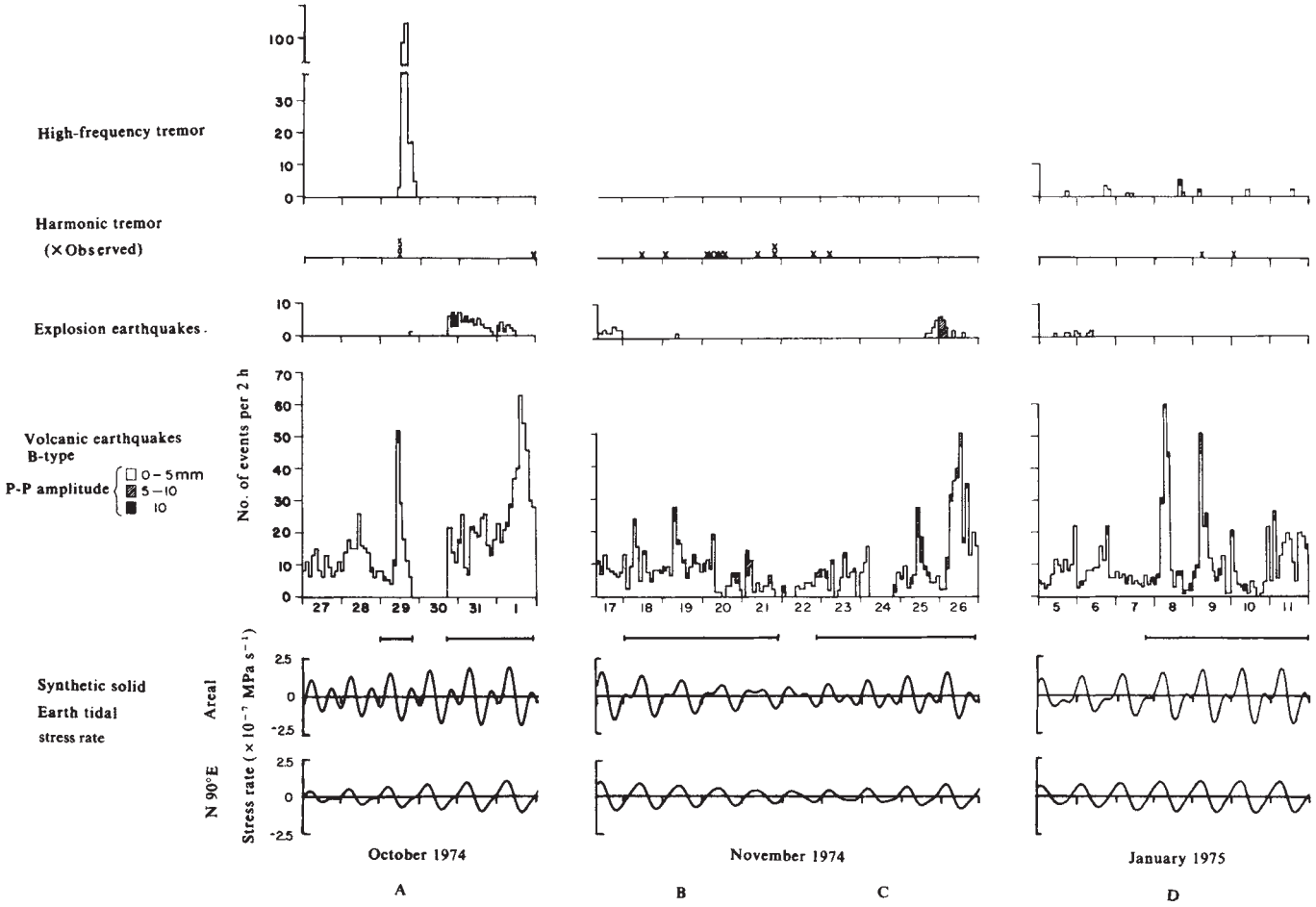

Fig. 3 Portions of histograms showing numbers of volcanic earthquakes of each type compared with synthetic solid earth tidal stress rate. A positive stress rate indicates increasing extensional stress. Note in particular the relation between the number of B-type earthquakes and tidal stress rate. A and C label pre-eruptive periods, while B and D label post-eruptive periods. During periods A and C peaks in the number of B-type earthquakes tend to occur at negative peaks in stress rate, while during periods B and D earthquakes occur at positive peaks in stress rate. See text for fuller explanation. The horizontal bars between the histograms and the tidal data show the portions of data actually used in the correlation calculations.

sequence is not shown; seismicity during this time period was the highest for the whole 7-month study period, and for reasons given below the results are less reliable. The results given in Table 2 show no statisticially significant correlation with tidal stress rate for either non-eruptive or eruptive seismicity. However, pre-eruptive and post-eruptive seismicity do show statistically significant correlations between the number of B-type volcanic earthquakes and the solid earth tidal stress rate for certain azimuths (Fig. 4). During pre-eruptive and post-eruptive periods earthquakes tend to occur at the times of tidal zero-crossings, that is when the rate of change of the tidal stress is most rapid. During pre-eruptive periods the correlation is negative: B-type earthquakes tend to occur at the time of most rapid increase in compressional tidal stress. For post-eruptive periods the correlation is positive: earthquakes tend to occur at the time of most rapid increase in extensional tidal stress. Table 2 shows a small but representative sample of the computed correlation data: estimates of correlation coefficients of regression, normalized slopes (that is, numbers of earthquakes per unit stress rate) and the confidence level of the correlation (the probability that the true correlation is greater than zero) are listed. We find that correlations with horizontal stress rate are better for azimuths from 75° to 105° than for other azimuths; correlations with volumetric (or areal) stress are similar to the best horizontal stress correlations.

Discussion

Ryall *et al.*[16] stated three criteria that should be met to evaluate optimally a tidal correlation: a statistically significant number of events, a limited focal region, and a relatively constant character of accumulated strain in the region, as evidenced by focal mechanism study of the earthquakes. The first two conditions are met at Pavlof Volcano. Focal mechanisms could not be determined for the volcanic earthquakes because (1) it is nearly impossible for volcanic earthquakes to determine polarity of the emergent first arrivals, and (2) only one station was in existence at the time of this sequence of events; however, the signal characteristics are remarkably similar and are consistent with a relatively constant mechanism. Several other factors are important: the eruption was small, hence processes were smooth and slow rather than catastrophic; except for one time period (16–25 December) the seismicity was low enough that there was virtually no overlap problem in reading records; and the earthquakes themselves were small, thus the tidal stresses may have attained a larger fraction of the presumed stress drops ($\approx$ a few bars) of the earthquakes than is the case for catastrophic events.

Our data are insufficient to determine unambiguously the focal process responsible for causing the earthquakes. Two processes are most likely; mode I (tensional) cracks and mode II (shear) cracks, which are both thought to occur as a result of magma injection into the volcanic pile. For the same crack geometry, however, the two processes would require different orientations of the principal stress axes to enhance most crack growth, or, vice versa, for a given stress system the two types of cracks most likely to be activated would be oriented at different azimuths. Our correlation data suggest a preferred orientation of cracks, but we cannot determine this orientation uniquely. Determinations of maximum horizontal compressive tectonic

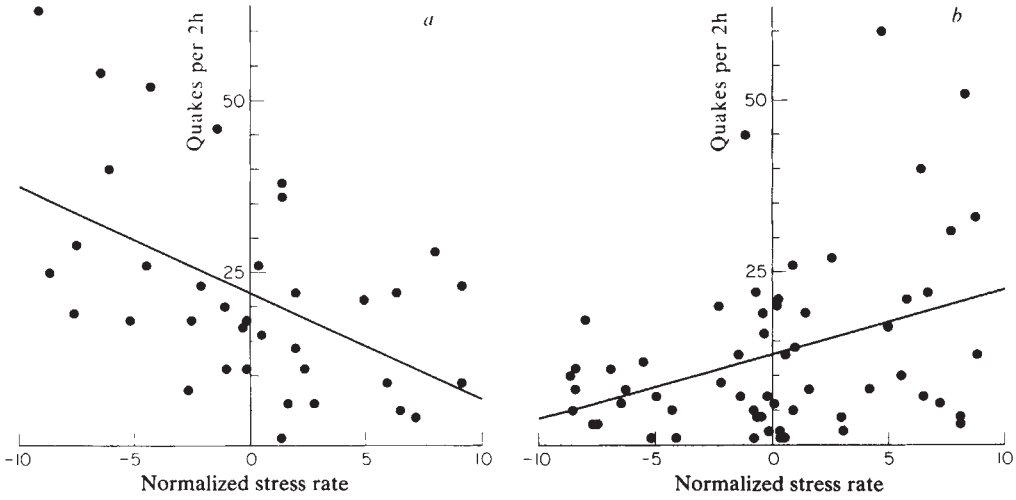

Fig. 4 Linear regression fits between earthquake frequency and stress rate. *a*, The data for a pre-eruptive period where the correlation is negative. The correlation coefficient is 0.51, and is >0 at the 99.9% confidence level. *b*, A post-eruptive period where the correlation is positive. The correlation coefficient is 0.37, and is >0 at the 99% confidence level.

stress[17,18] and the azimuth of relative plate convergence of the North American and Pacific plates[19] suggest an azimuth for the P-axis of maximum compression of approximately 150° which may control preferred crack growth in this direction if tensile cracks dominate, or at some angles ±45° from this azimuth if shear cracks dominate. This discussion does not consider pore pressure variations, which could change the effective stress significantly.

We tentatively interpret the change in sign of the correlation in terms of inflation and deflation of the volcano before and after eruptions, respectively. Some volcanoes tend to inflate before and deflate after eruptions[7,20], presumably due to buoyant forces exerted by magma on the volcanic edifice as the magma migrates through dykes, but no geodetic data are available for Pavlof to confirm this hypothesis.

The tidal correlation applies only for a period of 3–4 days before and after explosive eruptions. As in previous studies[21] this implies that the volcano is sensitive to changes in ambient stress rate of $\sim 2.5 \times 10^{-7}$ MPa s^{-1} during the times when magma is near the Earth's surface. Other volcanoes have quite slow rates of tectonic stress accumulation before eruptions[20]. The time period of 3–4 days may represent the time of magma ascent from or descent to a shallow magma chamber.

Our results indicate that the earth tide may have an effect on certain aspects of volcanic activity at Pavlof. This paper is believed to be the first to show a tidal correlation whose polarity with respect to tidal phase varies systematically during a volcanic eruption.

We thank Juergen Kienle and John Davies for helpful discussions and for cooperation in acquiring and using the data, Roger Bilham and Klaus Jacob for critical review and helpful comments, Lynn Zappa for typing the manuscript and Kazuko Nagao for drafting some of the figures. This work was partially supported by the National Oceanic and Atmospheric Administration, the Department of Energy, and the NSF under contracts NOAA-03-5-022-70, DE ACO2 76ERO 3134, EAR 79-12960, and EAR 80-24006, respectively. Lamont-Doherty Geological Observatory contribution no. 3251.

Received 11 August; accepted 28 October 1981.

1. Hamilton, W. L. *J. geophys. Res.* **78**, 3363–3375 (1973).
2. Klein, F. W. *Geophys. J. R. astr. Soc.* **45**, 245–295 (1976).
3. Golombek, M. P. & Carr, M. J. *J. Volcan. geotherm Res.* **3**, 299–307 (1978).
4. Martin, D. P. thesis, Mich. Tech. Univ. (1979).
5. Dzurizin, D. *Geophys. Res. Lett.* **7**, 925–928 (1980).
6. Knopoff, L. *Bull. seis. Soc. Am.* **54**, 1865–1870 (1964).
7. Minakami, T. *Bull. Earthq. Res. Inst.* **38**, 497–544 (1960).
8. Kennedy, G. C. & Waldron, H. H. *Bull. U.S. geol. Surv.* 1028-A, 1–19 (1955).
9. Johnston, M. J. S. & Mauk, F. J. *Nature* **239**, 266–267 (1972).
10. Shimozuru, D. *UNESCO Earth. Sci. Monogr.* No. 8, 19–45 (1971).
11. Minakami, T. *Devl. Solid Earth Geophys.* **6**, 313–333 (1974).
12. Longman, I. M. *J. geophys. Res.* **64**, 2351–2355 (1959).
13. Farrell, W. E. *Rev. Geophys.* **10**, 761–797 (1972).
14. Schwiderski, E. W. *Rev. Geophys.* **18**, 243–268 (1980).
15. Berger, J. & Beaumont, C. *Bull. seis. Soc. Am.* **66**, 1821–1846 (1976).
16. Ryall, A., Van Wormer, J. D. & Jones, A. E. *Bull. seis Soc. Am.* **58**, 215–248 (1968).
17. Nakamura, K. *J. Volcan. geotherm. Res.* **2**, 1–16 (1977).
18. Nakamura, K., Jacob, K. & Davies, J. N. *Pageophysics* **115**, 87–112 (1977).
19. Minster, J. B. & Jordan, T. H. *J. geophys. Res.* **83**, 5331–5354 (1978).
20. Fiske, R. S. & Kinoshita, W. T. *Science* **165**, 341–349 (1969).
21. Mauk, F. J. & Johnston, M. J. S. *J. geophys. Res.* **78**, 3356–3362 (1973).

Lithospheric studies based on holographic principles

P. Troitskiy*, E. S. Husebye† & A. Nikolaev*

* Academy of Science, Institute of Physics of the Earth, Moscow, USSR
† NTNF/NORSAR. Post Box 51, N-2007 Kjeller, Norway

Earth holography was applied to Norwegian Seismic Array (NORSAR) earthquake P-wave recordings. Simulation of the NORSAR sensor configuration indicates that a satisfactory reconstruction of the essential features of an embedded body is feasible with a depth resolution which seems to be better than that attained using more traditional time and amplitude inversion schemes. The earth holography concept was tested using NORSAR recordings of three deep earthquakes at teleseismic distances. The results indicate lithospheric heterogeneous bodies with a significant vertical extent. The most pronounced scattering features of these inhomogeneities are located at depths around 100, 148 and 212 km.

DETAILED mapping of subsurface geological structures is important both for exploration for natural resources and for a better understanding of tectonic processes. The best tools are those tied to seismic wave analysis in view of the very short wavelengths involved compared with other geophysical investigations. During the 1970s two novel approaches were introduced: (1) the scattering approach using the concept of an isotropic random medium with a prescribed statistical velocity

0028-0836/81/510618—06$01.00